EUROFUSION WPS1-PR(15) 14316

A. Langenberg et al.

Forward Modeling of X-ray Imaging Crystal Spectrometers within the Minerva Bayesian Analysis Framework

Preprint of Paper to be submitted for publication in
Fusion Science and Technology

This work has been carried out within the framework of the EUROfusion Consortium and has received funding from the Euratom research and training programme 2014-2018 under grant agreement No 633053. The views and opinions expressed herein do not necessarily reflect those of the European Commission.

Forward Modeling of X-ray Imaging Crystal Spectrometers within the Minerva Bayesian Analysis Framework

A. Langenberg,* J. Svensson, H. Thomsen, R. Burhenn, and R.C. Wolf
Max-Planck-Institut für Plasmaphysik, 17491 Greifswald, Germany

O. Marchuk
Forschungszentrum Jülich GmbH, Institut für Energie- und Klimaforschung - Plasmaphysik, 52425 Jülich, Germany
(EUROfusion Collaboration)

N.A. Pablant
Princeton Plasma Physics Laboratory, Princeton, NJ, USA
(Dated: July 23, 2015)

Two x-ray imaging crystal spectrometer systems, HR-XIS and XICS, are currently being prepared for commissioning at the stellarator Wendelstein 7-X (W7-X). Both are expected to be ready for the first plasma operation in 2015. The spectrometers will provide line integrated measurements of basic plasma parameters like ion and electron temperatures (T_e, T_i), plasma rotation (ϕ_{rot}) and argon impurity densities. A forward model based on the designed installation geometries of both spectrometers has been performed using the Minerva Bayesian Analysis framework. This model allows to create synthesized data given radial profiles of plasma parameters for a wide range of different scenarios. For the simulation of line integrated spectra as measured by the (virtual) detector, the geometry and Gaussian detection noise is assumed. The inference of line integrated plasma parameters is done within the framework using the maximum posterior method for an estimation of the plasma parameters from noisy spectral data. Capabilities and limitations of the model and method will be discussed through examples of several synthesized data of different plasma parameter profiles.

I. INTRODUCTION

X-ray imaging crystal spectrometers have developed to a standard diagnostic for providing line integrated measurements of impurity ion and electron temperatures (T_i, T_e), poloidal and toroidal plasma rotation $v_{rot}^{pol/tor}$, and impurity densities n_Z and have been operated successfully at several fusion experiments [1–6]. In these spectrometers, x-rays emitted from the plasma are imaged via a spherical bent crystal onto a 2D detector unit, monitoring a 2D intensity pattern with energy resolution in horizontal and spatial resolution in vertical direction. A spectral fit of line integrated data give access to above mentioned plasma parameters.
In this work, a full forward modeling of the High Resolution X-ray Imaging Spectrometer (HR-XIS) and the X-ray Imaging Crystal Spectrometer (XICS), currently assembled at W7-X, has been performed in the Minerva Bayesian Analysis framework (section II) to validate the expected performance of both spectrometer systems assuming standard as well as advanced plasma scenarios (section III A, B). In addition, a fast spectral fitting routine for inference of line integrated plasma parameters have been carried out. Synthesized data created by a forward modeling of XICS have been used to test the accordance of line integrated T_e and T_i values with the actual temperature profiles (section III C).

* andreas.langenberg@ipp.mpg.de

II. FORWARD MODELING

A forward modeling of the HR-XIS and XICS diagnostics has been carried out in the *Minerva Bayesian Analysis framework* (MBAF) [7]. The framework proved to be a comprehensive and universal tool for modeling a large variety of different diagnostics [8–11]. It provides several standard routines for spectral emission calculations, line of sight integrations, implementation of VMEC calculations *etc.*
Within this section, a graphical model for modeling measured data of the XICS and HR-XIS diagnostics, assumed temperature and density profiles of several plasma scenarios, and a graphical model for a spectral fitting of measured spectra will be discussed in more detail.

A. Graphical Model

In the MBAF, physics parameters and physical models are expressed in a graphical model. Here, model parameters $\boldsymbol{N}$ (blue ellipses), physical models (rectangles), and modeled data $\boldsymbol{D^*}$ (gray ellipses, *cf.* Fig.1) are represented as nodes and linked to each other, defining the dependencies between model parameters and measured data: $f(\boldsymbol{N}) = \boldsymbol{D^*}$. The use of a graphical model allows for a high flexibility regarding modifications or upgrades of the forward model. Therefore, even complex rearrangements of the forward model like switching between different spectral emission models, changing line

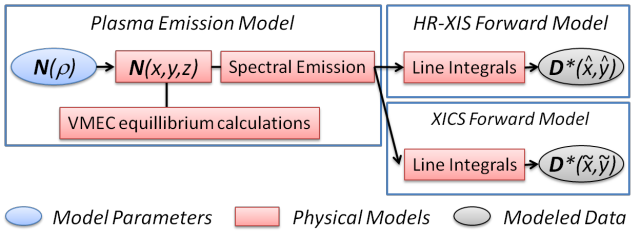

FIG. 1. Simplified graphical model of an entire forward model for the HR-XIS and XICS diagnostics.

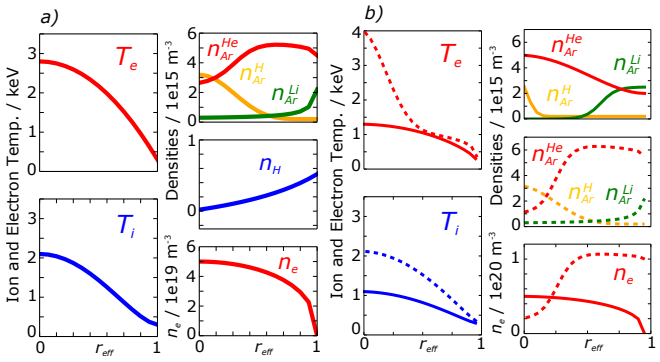

FIG. 2. Assumed temperature and density profiles for calculating the spectral emission of He-like Ar for: a) A standard plasma scenario. b) Low heating power (solid lines) and central density hole scenarios (dotted lines).

of sight geometries or adding observations from other diagnostics can be handled easily by exchanging or adding individual nodes [7].

A simplified scheme of the graphical model used for modeling the x-ray imaging crystal spectrometers is shown in Fig.1. It is split into a physics model (plasma emission model) and two diagnostic models (HR-XIS and XICS forward model). Within the physics model the spectral emission of selected impurities as *e.g.* He-like Ar can be modeled in 3D space. Input model parameters for evaluation of the spectral emission are radial profiles of ion and electron temperatures T_i and T_e, the electron density n_e, different ionization stages (H-, He-, and Li-like) of Ar $n_{Ar}^{H/He/Li}$, and the neutral hydrogen density n_H, all represented by the blue node in Fig.1. Assuming constance on magnetic flux surfaces, the model parameters are parameterized as a function of the effective radius $\boldsymbol{N}(\rho)$, with ρ being the square root of magnetic flux ψ, normalized to the magnetic flux of the last closed flux surface ψ_{LF}: $\rho = \sqrt{\psi/\psi_{LF}}$.

Mapping the 1D profiles $\boldsymbol{N}(\rho)$ into 3D space $\boldsymbol{N}(x, y, z)$ is done using equilibrium flux surfaces $\psi_n(x, y, z)$ as given by VMEC calculations [12], with spatial coordinates x, y, and z. Finally, the spectral emission is modeled along lines of sight as defined in the diagnostic model, yielding line integrated synthesized data on the detector (gray nodes in Fig.1) for both HR-XIS and XICS diagnostics. Here, $\hat{x}, \hat{y}$ and $\tilde{x}, \tilde{y}$ denote the detector pixel coordinates.

B. Model Inputs

For a proper modeling of spectra emitted from highly charged ions, the following atomic effects have been considered in the spectral emission model: A. Excitation of the He-like ground state, B. dielectronic recombination, C. recombination of H-like ions, D. inner-shell excitation and ionization, and E. charge exchange recombination with neutral background gas hydrogen [5]. The later effect is of particular importance in case of low electron temperatures and a high neutral hydrogen background at the plasma edge as well as for neutral beam injection [13, 14].

In Fig.2, temperature and density profiles of three different plasma scenarios are shown that in the following will be referred to as *assumed* model parameters utilized for the forward modeling of *synthesized* data.

The set of temperature and density profiles in Fig.2 a) corresponds to an expected standard plasma scenario of W7-X. Assumed electron and ion temperature and electron density profiles have been set similar to profiles derived by neoclassical calculations [15], impurity density profiles mimic measured profiles from Alcator C-Mod [3]. Solid lines in Fig.2 b) represent a set of plasma parameters expected for the first operational phase of W7-X. Since the machine will run in a limiter configuration without a divertor unit, for machine safety reasons short time discharges (several 100 ms) with moderate heating power ($\approx$ 0.5 MW) and temperatures ($T_e < 3$ keV) are going to be realized. Note that due to the low temperatures, the maxima of fractional abundances for the ionization stages of Ar are shifted towards the plasma center. In particular, the hollow n_{Ar}^{He} profile of the standard scenario changes to a peaked profile, see Fig.2 a) and b).

Dotted lines in Fig.2 b) show a set of plasma parameters that are predicted in large stellarators in case of non optimized particle refilling rates [16]. Here, central electron temperatures are highly peaked up to 4 keV combined with a hollow electron density profile. Additionally, the high central electron temperature will cause the ionization stage of He-like Ar to vanish close to the plasma center, yielding a hollow n_{Ar}^{He} profile as shown in Fig2 b). Such an impurity hole scenario, as observed in LHD [4], represents a challenging configuration for x-ray imaging spectrometer systems regarding the inference of plasma parameter profiles, as will be discussed in section III C.

C. Spectral Fitting

In order to infer plasma parameters from measured line integrated spectra, a simplified forward model for modeling a single spectrum given the plasma parameters has been defined in Fig.3. In contrast to the spectrometers forward model, here model parameters $\boldsymbol{N}$ (blue nodes in Fig.3) enter the local emission model as single values and not as radial profiles $\boldsymbol{N}(\rho)$, respectively. Hence, the modeled spectrum (gray node in Fig.3) corresponds to a

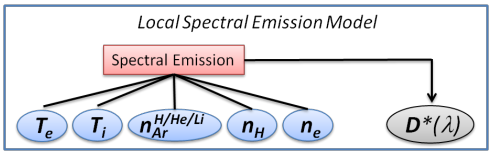

FIG. 3. Graphical model for modeling a single emission spectrum, given the plasma parameters.

local spectral emission, given the model parameters $\boldsymbol{N}$.

For a spectral fitting of synthesized data, model parameters are varied with respect to an optimal match between modeled and synthesized spectra via maximization of the posterior $\boldsymbol{P(N|D)}$, using Bayes theorem:

$$\boldsymbol{P}(\boldsymbol{N}|\boldsymbol{D}) = \boldsymbol{P}(\boldsymbol{D}|\boldsymbol{N})\boldsymbol{P}(\boldsymbol{N})/\boldsymbol{P}(\boldsymbol{D}) \quad (1)$$

with the *likelihood distribution* $\boldsymbol{P(D|N)}$, representing the probability of observed data for given parameters $\boldsymbol{N}$, the prior distribution $\boldsymbol{P(N)}$ incorporating any knowledge on the model parameters before the measurement took place, and a normalization constant $\boldsymbol{P(D)}$.

Applied to spectra observed on a CCD camera with a number of pixels N_{pix}, the likelihood is defined as

$$\boldsymbol{P}(\boldsymbol{D}|\boldsymbol{N}) = \prod_{p=0}^{N_{pix}-1} \frac{1}{\sqrt{2\pi}\sigma_p} exp\left(-\frac{(\boldsymbol{D}_p^* - \boldsymbol{D}_p)^2}{2\sigma_p^2}\right). \quad (2)$$

Here, a normal distribution with standard deviation σ_p is assumed for the photon statistics [17]. The predicted and observed numbers of counts are $\boldsymbol{D}_{\boldsymbol{p}}^*$ and $\boldsymbol{D}_{\boldsymbol{p}}$ for each pixel $\boldsymbol{p}$.

Since the synthesized spectra of the spectrometers are line integrated along lines of sight, fitted plasma parameters also correspond to line integrated values.

III. RESULTS AND DISCUSSION

A. Modeling of the HR-XIS and XICS Diagnostics

The results of the forward modeling for the HR-XIS and XICS diagnostics are presented in Fig.4. For the forward modeling, assumed temperature and density profiles shown in Fig.2 a) have been used. In Fig.4 a) and c), the designed viewing geometries for both spectrometers are shown in green shaded areas together with the magnetic flux surfaces.

Both spectrometers lines of sight cross the plasma in a poloidal cross section of bean shaped magnetic flux surfaces but at different toroidal angles of $\phi = 7.38°$ and $\phi = 159.09°$ for HR-XIS and XICS, respectively. Since the HR-XIS detector consists of six separate CCD detectors, its view field corresponds to 6 arrays of lines of sight as shown in Fig.4 a). The actual cone shaped lines of sight with a maximum vertical expansion of 2 cm have been approximated by line integrals with a horizontal resolution of 1 cm, equal to 100 points along each line of sight.

Magnetic flux surfaces in Fig.4 a) and c) shown for $\rho = 0.1 - 1.0$ correspond to VMEC calculations for a vacuum field of a W7-X standard configuration.

Synthesized data at the positions of the HR-XIS and XICS detectors are shown in Fig.4 b) and d). The detector system used for the HR-XIS consists of six *CCD30-11 deep depletion sensors, Marconi Applied Technologies, England*, each with 1024 x 256 pixels of 26 x 26 μm^2 pixel size and an image area of 26.6 x 6.7 mm^2. The XICS diagnostic is equipped with a *Pilatus 300K, Dectris inc., Switzerland* detector with 1475 x 195 pixels of 172 x 172 μm^2 pixel size and an image area of 251.4 x 33.5 mm^2. Corresponding to the detector units used in HR-XIS and XICS, a total amount of 1024 x (6 x 256) and 195 x 1475 pixels have been modeled in Fig.4 b) and d).

The 2D intensity patterns on the detectors of the HR-XIS and XICS diagnostic have been synthesized exemplarly for the spectral emission of He-like Ar. In order to simulate a realistic diagnostic environment, a typical statistical noise level with a signal to noise ratio (SNR) of 300 for the central and 15 for the edge line of sight [3] has been added to the spectra. Fig.4 e) shows line integrated spectra of the XICS diagnostic, averaged along the central and edge line of sight. Within the emission model, the main intense excitation lines (w, x, y, and z), dielectronic satellites up to n=4, and all inner shell excitation lines (like q and r) have been taken into account in the spectra as marked in Fig.4 e). Since also the imaging properties of the crystal have been added in the spectral emission model, focal lines on the detector are curved, yielding slight energy shifts between individual lines of sight as can be seen for the central and edge line of sight spectra in Fig.4 e). The shapes of spectral emission lines have been modeled as Voigt profiles, resulting from a Lorentzian contribution of the natural linewidth, a Gaussian contribution from Doppler broadening, and the instrumental profiles.

B. Synthesized XICS Data of Different Plasma Scenarios

To illustrate the impact of plasma parameters to measured spectra, the forward model has been used to create synthesized spectra of XICS for three different plasma scenarios with assumed plasma parameter profiles shown in Fig.2 a) and b). Fig.5 a)-c) shows synthesized spectra of a) standard, b) low temperature, and c) density hole plasma scenarios for the central and edge lines of sight of XICS.

The individual line intensity ratios as well as the overall

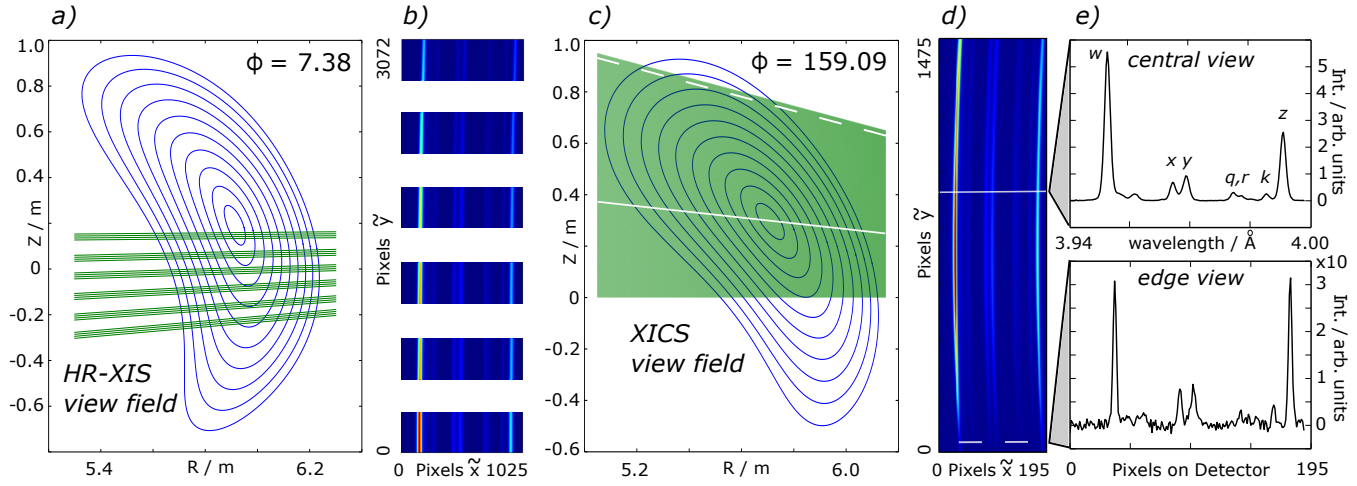

FIG. 4. Forward modeling of the HR-XIS and XICS diagnostics for spectral emission of He-like Ar: a) Magnetic flux surfaces and viewing geometry of HR-XIS in the poloidal cross section of the measurement. b) Modeled 2D intensity pattern on the 6 CCD detector units of HR-XIS. c) Magnetic flux surfaces and viewing geometry of XICS in the poloidal cross section of the measurement. d) Modeled 2D intensity pattern on the CCD detector unit of XICS. Solid and dashed lines correspond to central and edge lines of sight. The uppermost line of sight (edge view) corresponds to the lowest horizontal pixel array (dotted line) and vice versa. e) Synthesized spectra along the central and outermost line of sight with main intense w, x, y, and z emission lines and satellites q, r, and k.

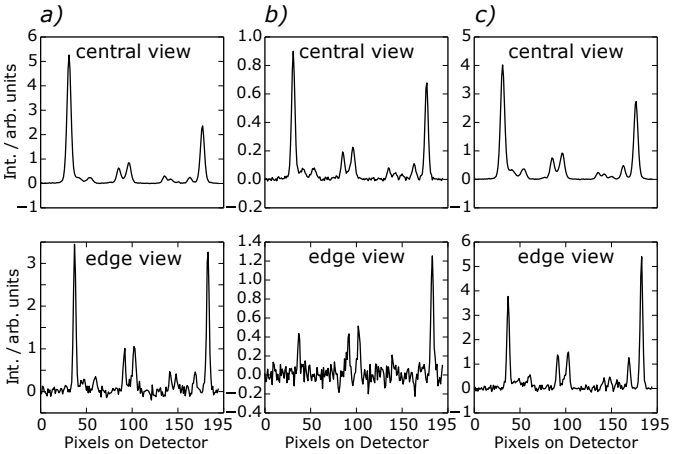

FIG. 5. Synthesized spectra along the central and outermost XICS line of sight for a) standard, b) low temperature, and c) density hole plasma scenarios.

intensities of spectral emission lines, especially of the w and z line, are mainly determined by the electron temperature while the linewidths change with the ion temperature. Therefore, radially decreasing electron and ion temperatures towards the edge result in reduced w/z line ratios, reduced overall line intensities, and narrower linewidths for the edge compared to the central line of sight spectra, as can be seen for all plasma scenarios in Fig.5 a) - c).

In spectra of the edge view for the low temperature and density hole scenario, Fig.5 b) and c), even an inverted w/z line ratio ($w/z < 1$) occurs. This effect is usually observed at the plasma edge at low electron temperatures [3, 13, 14] and is induced by charge exchange of neutral hydrogen background gas with H-like Ar [13]. For all plasma scenarios the same profile for the neutral hydrogen background has been assumed, see Fig.2 a).

Comparing spectra of the central view for the standard and density hole scenario, Fig.5 a) and c), shows a reduced w/z line ratio for the density hole case, indicating a lower central T_e value. However, the T_e profile of the density hole scenario is highly peaked and T_e in the center is about 1 keV higher than in the standard case. This effect of underestimated central temperatures, induced by the existence of hollow density profiles, will be discussed in more detail in the next section.

C. Inference of Line Integrated Ion and Electron Temperatures

For the inference of line integrated plasma parameters out of synthesized XICS data, the fitting routine described in section II C has been used. Since thereby just averaged plasma parameters, integrated along the lines of sight can be determined, these line integrated values are not expected to resemble the actual assumed plasma parameter profiles. However, since the assumed profiles are known, the accuracy of line integrated plasma parameters compared to the actual profiles can be evaluated for different plasma scenarios.

Assumed electron and ion temperature profiles (solid lines) are shown together with line of sight averaged values (dotted lines) in Fig.6 for a) standard, b) low temperature, and c) impurity density hole scenarios.

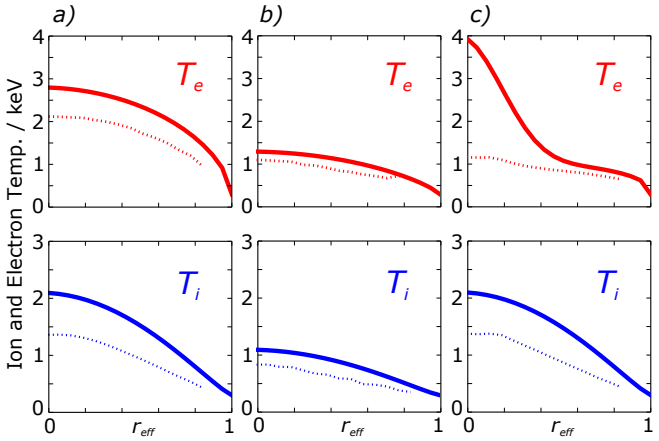

FIG. 6. Assumed electron and ion temperature profiles (solid lines) compared to line integrated values (dotted lines) inferred from synthesized spectra.

In the standard plasma scenario, line of sight averaged T_e and T_i values are systematically underestimated compared to the assumed profiles with maximum relative deviations in the plasma center of $\delta T_e = 0.25$ and $\delta T_i = 0.38$. Towards the plasma edge, line integrated temperature values gradually approach to the assumed profiles since the region of averaged flux surfaces decrease.
The accuracy of line integrated values is dominated by the shapes of T_e and n_{Ar}^{He} profiles that determine the spectral emission intensity along the effective radius. If both T_e and n_{Ar}^{He} profiles are peaked, the maximum weight of spectral emission is located in the plasma center, yielding a good approximation of line integrated T_e and T_i values compared to assumed profiles as shown in Fig.6 b). Here, the n_{Ar}^{He} profile has been assumed to be peaked due to the low central electron temperature, see Fig.2 b).
If in contrast the n_{Ar}^{He} profiles are hollow and close to zero in the plasma center as assumed in the impurity density hole scenario, the central spectral emission intensity will also be close to zero. Therefore, the peaked T_e profile is not resembled by the line integrated T_e values, shown in Fig.6 c).
Especially for hollow impurity density profiles, the inference of the actual plasma parameter profiles is required. This can be done in principle by using the full spectrometer forward model in Fig.1 for the inference of free parameters, defined as plasma parameter profiles, and will be discussed elsewhere [18].

IV. CONCLUSION

In this work, a forward modeling of two x-ray imaging spectrometer systems within the Minerva Bayesian Analysis framework has been presented. For different plasma scenarios, synthesized data created by forward modeling of XICS have been fitted with a local spectral emission model to infer line of sight averaged T_e and T_i values. Since the inference of line of sight averaged values has a fast performance with less than 10 seconds per detector image, it is appropriate for data analysis between plasma shots in the first operation phase of W7-X.
A comparison of line integrated T_e and T_i values to the actual profiles show a good agreement for peaked T_e and n_{Ar}^{He} profiles. In case of hollow impurity density profiles, line integrated temperatures are systematically underestimated and an inversion of line integrated values is required.

V. ACKNOWLEDGMENTS

This work has been carried out within the framework of the EUROfusion Consortium and has received funding from the Euratom research and training programme 2014-2018 under grant agreement No 633053. The views and opinions expressed herein do not necessarily reflect those of the European Commission.

[1] A. S. Rosen, M. L. Reinke, J. E. Rice, A. E. Hubbard, and J. W. Hughes, Journal of Physics B-atomic Molecular and Optical Physics **47**, 105701 (2014).
[2] S. G. Lee, J. G. Bak, U. W. Nam, M. K. Moon, Y. Shi, M. Bitter, and K. Hill, Review of Scientific Instruments **81**, 10E506 (2010).
[3] A. Ince-Cushman, J. E. Rice, M. Bitter, M. L. Reinke, K. W. Hill, M. F. Gu, E. Eikenberry, C. Broennimann, S. Scott, Y. Podpaly, S. G. Lee, and E. S. Marmar, Review of Scientific Instruments **79**, 10E302 (2008).
[4] N. A. Pablant, M. Bitter, L. Delgado-Aparicio, M. Goto, K. W. Hill, S. Lazerson, S. Morita, A. L. Roquemore, D. Gates, D. Monticello, H. Nielson, A. Reiman, M. Reinke, J. E. Rice, and H. Yamada, Review of Scientific Instruments **83**, 083506 (2012).
[5] O. Marchuk, *Modeling of He-like spectra measured at the tokamaks TEXTOR and TORE SUPRA*, Ph.D. thesis, Ruhr Universität Bochum (2004).
[6] P. Beiersdorfer, M. Bitter, M. J. May, and L. Roquemore, Review of Scientific Instruments **74**, Univ Wisconsin Madison; Amer Phys Soc, Div Plasma Phys; US DOE, Off FusEOLEOLEnergy Sci & Defense Sci (2003).
[7] J. Svensson and A. Werner, in *International Symposium on Intelligent Signal Processing-WISP* (2007) pp. 955–960.
[8] A. Langenberg, K. Hirsch, A. Lawicki, V. Zamudio-Bayer, M. Niemeyer, P. Chmiela, B. Langbehn, A. Terasaki, B. V. Issendorff, and J. T. Lau, Physical Review B **90**, 184420 (2014).

[9] O. Ford, *Tokamak Plasma Analysis through Bayesian Diagnostic Modelling*, Ph.D. thesis, University of London, Imperial College London (2010).
[10] O. Ford, J. Svensson, A. Boboc, and D. C. McDonald, Review of Scientific Instruments **79**, 10F324 (2008).
[11] J. Svensson and A. Werner, Plasma Physics and Controlled Fusion **50**, 085002 (2008).
[12] M. Drevlak, D. Monticello, and A. Reiman, Nuclear Fusion **45**, 731 (2005).
[13] J. E. Rice, E. S. Maramar, E. Källne, and J. Källne, Physical Review A **35**, 3033 (1987).
[14] T. Schlummer, O. Marchuk, D. Schultz, G. Bertschinger, W. Biel, D. Reiter, and the TEXTOR-Team, Journal of Physics B: Atomic, Molecular and Optical Physics **48**, 144033 (2015).
[15] Y. Turkin, C. D. Beidler, H. Maassberg, S. Murakami, V. Tribaldos, and A. Wakasa, Physics of Plasmas **18**, 022505 (2011).
[16] H. Maassberg, C. D. Beidler, and E. E. Simmet, Plasma Physics and Controlled Fusion **41**, 1135 (1999).
[17] J. Svensson and R. König, in *32nd EPS Conference on Plasma Physics* (2005) p. 5.087.
[18] A. Langenberg, J. Svensson, H. Thomsen, R. Burhenn, R. C. Wolf, O. Marchuk, and N. Pablant, To be published.